CHEMISTRY OF MATERIALS
Cite This: Chem. Mater. 2019, 31, 4184−4194
Article
pubs.acs.org/cm

Ferroelectric, Optical, and Photovoltaic Properties of Morphotropic Phase Boundary Compositions in the $PbTiO_3$−$BiFeO_3$−$Bi(Ni_{1/2}Ti_{1/2})O_3$ System

Liyan Wu,[†] Adrian Podpirka,[‡] Jonathan E. Spanier,[‡] and Peter K. Davies*[,†]

[†]Department of Materials Science and Engineering, University of Pennsylvania, Philadelphia, Pennsylvania 19104, United States
[‡]Department of Materials Science and Engineering, Drexel University, Philadelphia, Pennsylvania 19104, United States

Supporting Information

ABSTRACT: Ferroelectrics can exhibit the bulk photovoltaic effect (BPVE), which enables a switchable photoresponse and above-band-gap open-circuit voltages (V_{oc}). For these systems a large remnant polarization (P_r) combined with a narrow band gap (E_g) is believed to be critical in optimizing the photovoltaic performance. Here we investigate the $PbTiO_3$−$BiFeO_3$−$Bi(Ni_{1/2}Ti_{1/2})O_3$ system which exhibits a large bulk P_r and a tunable narrow E_g. To optimize the ferroelectric polarization, ceramic samples were prepared in the vicinity of the ternary morphotropic phase boundary (MPB), and their photovoltaic properties were characterized over a broad range of optical wavelengths. MPB compositions with a direct optical gap ranging from 2.25 to 2.85 eV and P_r = 32−39 $\mu C/cm^2$ show a BPVE with V_{oc} = 6 V at room temperature and a wavelength-dependent switchable photoresponse. Under 1 sun AM 1.5 G illumination the short-circuit photocurrent (j_{sc}) increased by an order of magnitude as E_g was lowered from 2.85 to 2.25 eV, with ∼0.1 $\mu A/cm^2$.

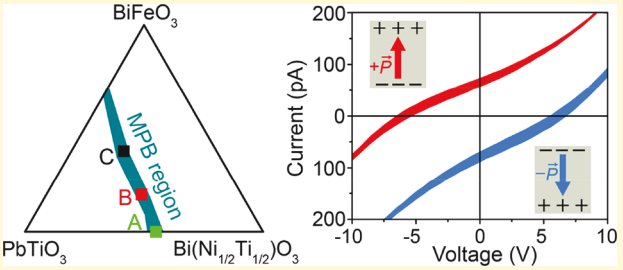

1. INTRODUCTION

Ferroelectric materials are characterized by their switchable spontaneous polarization which enables important technological applications such as dielectric capacitors, piezoelectric sensors and actuators, and ferroelectric random-access memories.[1] The discovery of magnetoelectric coupling in systems such as $BiFeO_3$ and $TbMnO_3$ has also led to their exploration as multiferroic materials.[2,3] The photovoltaic effect in ferroelectrics, which remained an academic curiosity since its discovery in the 1970s,[4−7] has recently attracted considerable attention due to the growing demand for higher efficiency photovoltaic materials. The breaking of inversion symmetry in ferroelectrics can allow the separation of photoexcited charge carriers throughout the entire sample with above-band-gap photovoltages and potential power conversion efficiencies beyond the Shockley−Queisser limit.[8,9] The ferroelectric polarization can also induce interfacial electric fields along domain walls and/or electrode interfaces which provide additional degrees of freedom in controlling the photovoltaic properties.[10−12]

Despite their potential in solar energy conversion, most ferroelectric oxides have wide band gaps (E_g > 3.0 eV) that severely limit the fraction of the visible spectrum absorbed and yield very low power conversion efficiencies. Therefore, the ability to engineer a tunable narrow band gap is critical in improving the photovoltaic performance of oxide ferroelectrics and in enabling their application in photoelectronic devices. Although only a lack of inversion symmetry is necessary for a bulk photovoltaic effect (BPVE) which consists of shift and ballistic mechanisms,[8,13,14] a sizable polarization is desirable for manipulating the polarity of the BPVE and enhancing the interfacial electric fields. In displacive ferroelectrics a large polarization is normally associated with a high Curie temperature (T_C), which is also important for high-temperature applications and the environmental stability of a photovoltaic device. Therefore, systems with a tunable and narrow E_g and a large remnant polarization (P_r) are of interest in providing a platform for understanding the BPVE.

The BPVE effect in $BiFeO_3$, one of the few examples that combines a relatively low E_g (2.7 eV) with a large spontaneous polarization (∼60 $\mu C/cm^2$ along the pseudocubic (001) direction), has been explored in thin films and single crystals.[15,16] However, the exploration of the photovoltaic effect in $BiFeO_3$ in a ceramic form is limited by the difficulty in obtaining single phase, insulating ceramic samples. Several efforts have been made to tailor the properties of other ferroelectric oxides for photovoltaic applications by lowering their band gaps through chemical substitution[17−21] and/or introducing cation ordering.[22−25] A summary of the literature data for these systems provided in Table 1, and the observed P_r is plotted with respect to the E_g in Figure 1. Significant reductions in the band gaps of conventional ferroelectric oxides

Received: March 12, 2019
Revised: May 15, 2019
Published: May 16, 2019

DOI: 10.1021/acs.chemmater.9b00996
Chem. Mater. 2019, 31, 4184−4194

Table 1. Literature Data of Ferroelectric Oxides Studied for Photovoltaic Application[a]

chemical composition	E_g (eV)	P_r (μC/cm^2)	E_g tunability (eV)	T_C (K)	thin film or bulk	structure	ref
$BiFeO_3$	2.7	60	N/A	1100	s.c. and t.f.	Rhmb. prvsk.	2,12,33,35
$LiNbO_3$	3.78	71	N/A	1483	s.c.	$LiNbO_3$-type	34
$KBiFe_2O_5$	1.6	3.73	N/A	780	s.c.	Brownmillerite phase	29,30
$BaTiO_3$	3.3	25	N/A	400	s.c. and t.f.	Tetra. prvsk.	13,14,39
La-doped $BiFeO_3$ (**La-BF**)	2.32	60	N/A	713	t.f.	Rhmb. prvsk.	36
$Bi(Fe_{1-x}Co_xO)_3$ (**Co-BF**)	2.3	60	0.4	N/A	t.f.	Rhmb. prvsk.	37
$Bi_{0.925}Sm_{0.075}Fe_{0.95}Co_{0.05}O_3$ (**Sm,Co-BF**)	2.27	60	N/A	N/A	t.f.	Tetra. prvsk.	38
$Bi_4Ti_3O_{12}$−$LaCoO_3$ superlattice (**BiT-LC**)	2.65 to 3.55	15	0.9	N/A	t.f.	Aurivillius phase	18
$Bi_5FeTi_3O_{15}$	2.68	10 to 15	N/A	1030	t.f.	Aurivillius phase	40
$Bi(Fe_{1/2}Cr_{1/2})O_3$ (**BFCO**)	1.4 to 2.3	5 to 45	0.9	N/A	t.f.	Double prvsk.	23
(Co,Fe)-doped $Bi_{3.25}La_{0.75}Ti_3O_{12}$ (**BLCFT**)	2.48	2.6	N/A	N/A	t.f.	Aurivillius phase	41
$LuMnO_3$	1.55	5	N/A	N/A	t.f.	Hexagonal manganite	26
$YbFeO_3$	2	4	N/A	N/A	t.f.	Hexagonal ferrites	28
$(Pb_{0.97}La_{0.03})(Zr_{0.52}Ti_{0.48})O_3$ (**PLZT3/52/48**)	3.4	35 to 45	N/A	N/A	b.c.	Tetra. prvsk.	42,43
$Ba_{1-x}(Bi_{0.5}Li_{0.5})_xTiO_3$ (**BBLT**)	3.2	8	N/A	352	b.c.	Tetra. prvsk.	44
$0.9BaTiO_3$-$0.1Ba(Ni_{1/2}Nb_{1/2})O_{3-\delta}$ (**BTNN**)	1.5	4	N/A	N/A	b.c.	Tetra. prvsk.	21
$BaTi_{0.925}(Mn_{1/2}Nb_{1/2})_{0.075}O_3$ (**BTMN**)	1.66	15	N/A	345	b.c.	Tetra. prvsk.	45
$(1-x)KNbO_3$-$xBa(Ni_{1/2}Nb_{1/2})O_{3-\delta}$ (**KBNN**)	1.1 to 3.8	0 to 5 (at 77K)	2.7	736	b.c.	Orth. prvsk.	17,46
$0.65PbTiO_3$-$0.35Bi(Ni_{2/3+x}Nb_{1/3-x})O_{3-\delta}$ (**PT-BNN**)	2.9 to 3.0	33	0.1	533	b.c.	Tetra. prvsk.	19
$(1-x)(Na_{1/2}K_{1/2})NbO_3$-$xBa(Ni_{1/2}Nb_{1/2})O_{3-\delta}$ (**KNBNN**)	1.50 to 1.63	0 to 11	0.13	N/A	b.c.	Orth. prvsk.	47
$Sr_{1-x}Bi_{2+x}Nb_{2-x}Ni_xO_{9-x}$ (**SBNN**)	2.25 to 2.7	1.1 to 2.7	0.45	N/A	b.c.	Aurivillius phase	20

[a]s.c. = single crystal, t.f. = thin film, b.c. = bulk ceramic, Rhmb. = rhombohedral, Tetra. = tetragonal, Orth. = orthorhombic, and prvsk. = perovskite.

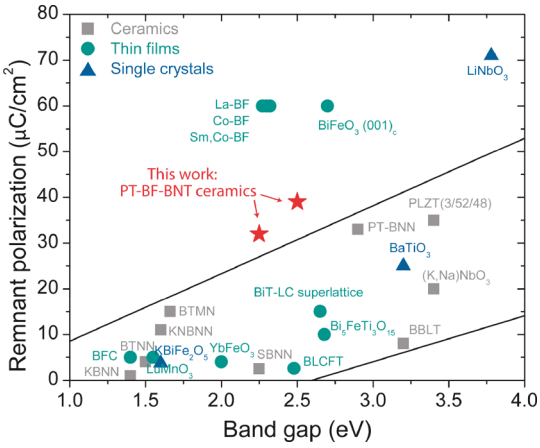

Figure 1. Summary of experimentally measured band gaps and remanent polarization of ferroelectric oxides designed for photovoltaic applications. References are summarized in Table 1.

have been reported for systems such as $Ba(Ni_{1/2}Nb_{1/2})O_{3-\delta}$ doped $KNbO_3$ and Ni/Nb-substituted $BaTiO_3$ where the lowest E_g values (1.4−1.6 eV) are comparable to those of traditional semiconductors.[17,21] However, the P_r of the substituted compounds are significantly inferior to that of the undoped ferroelectric end-member due to the replacement of the ferroelectrically active d^0 cations by inactive d^n cations and leakage caused by defects such as oxygen vacancies. Multiferroic oxides such as hexagonal manganites/ferrites[26−28] and the non-perovskite phase $KBiFe_2O_5$[29,30] have also been shown to have band gaps suited to photovoltaic applications; however, the polarization of those systems is quite small ($\leqslant$5 μC/cm^2).[31,32] Most systems show a clear empirical trend of a reduction in P_r with the narrowing of E_g (see the enclosed region in Figure 1). Although $Bi_4Ti_3O_{12}$−$LaCoO_3$ superlattices and $PbTiO_3$−$Bi(Ni_{2/3}Nb_{1/3})O_3$ solid solutions are examples where a substantial polarization (15 and 33 μC/cm^2, respectively) is retained, the chemical substitution only produces a very limited reduction in E_g.[18,19] The ability to induce a continuous variation in E_g, while retaining a bulk polarization, is also important in designing multilayer solar cells that could utilize the entire solar spectrum; this has been successfully achieved in $Bi(Fe_{1/2}Cr_{1/2})O_3$ epitaxial thin films through processing-induced B-site ordering.[23] However, the P_r in this system also drops significantly from 45 to 5 μC/cm^2 as the E_g is reduced.

In this paper we explore potential new photovoltaic materials, preparable in ceramic form, that combine a large polarization with a reduced and tunable band gap. In an attempt to maintain a high polarization, we investigated a (Pb, Bi)-based pseudoternary system where one of the component binaries, $PbTiO_3$−$BiFeO_3$ (PT−BF), exhibits enhanced tetragonality with a high T_C. BF is one of a few solid solution additives that increase the c/a ratio of PT,[48−51] and the substitution also reduces the band gap.[52] However, highly tetragonal PT−BF ceramics are not practical for bulk ferroelectric applications due to the large coercive field and the large internal strains accompanying the paraelectric-to-ferroelectric transition which cause cracking during cooling.[53] To mitigate these issues, we focused on solid solutions of PT−BF with a third component, $Bi(Ni_{1/2}Ti_{1/2})O_3$ (BNT), that could induce an MPB and maintain a high T_C and low band gap. The choice of BNT was guided by previous theoretical[32,54] and experimental[17,19−21,47] studies that show Ni^{2+} is effective in lowering the E_g of titanate and niobate perovskites, while the occupancy of Ti^{4+} on the remaining B-sites and Bi^{3+}

DOI: 10.1021/acs.chemmater.9b00996
Chem. Mater. 2019, 31, 4184−4194

on the A-sites can promote polar distortions. Although pure BNT can only be stabilized in a perovskite form at high pressure,[55] an extensive range of solid solutions with PT up to 65% BNT can be prepared at 1 atm. The previous studies also showed the PT−BNT pseudobinary forms an MPB between ∼51 and 55% BNT with a T_C (≈670 K) that is higher than the $Pb(Zr,Ti)O_3$ system;[56−59] there are no reports on the optical absorption properties of this system.

Here we investigate the structural, ferroelectric, and optical properties of the PT−BF−BNT ternary system and the photovoltaic response of compositions at the MPB. The ternary shows band gaps ranging from 3.2 to 1.75 eV, and the MPB compositions retain a substantial P_r (>32 $\mu C/cm^2$) with switchable, linear photovoltaic $I-V$ responses and above-band-gap open-circuit voltages (V_{oc}). The wavelength dependence of the light-induced response shows a correlation between the photocurrent and the band gap and under 1 sun AM 1.5 G illumination the photovoltaic performance (e.g., V_{oc} = 5 V; j_{ph} = 0.09 $\mu A/cm^2$) of the MPB compositions exceeds most previously reported ferroelectric oxide ceramics.

2. EXPERIMENTAL PROCEDURES

Samples in the PT−BF−BNT ternary system were prepared by conventional solid-state synthesis. Analytical grade starting powders of PbO, Bi_2O_3, TiO_2, Fe_2O_3, and NiO were weighed stoichiometrically and mixed by ball milling for 6 h. The mixtures were pressed into pellets and calcined between 750 and 850 °C for 6 h through multiple firings with intermediate grinding to promote homogeneity. After ball milling for 12 h, the calcined powders were pressed into 3 mm thick, 8 mm diameter pellets in a uniaxial press, surrounded by sacrificial powder of the same composition, and then sintered in a platinum crucible at temperatures between 1000 and 1050 °C, depending on the specific composition, for 2 h. The sintered pellets were cut into 0.5 mm thick slices or crushed into a powder for subsequent characterization. X-ray diffraction (XRD) patterns of powder samples were collected on an X-ray diffractometer (Rigaku GiegerFlex D/Max-B) using Cu Kα radiation generated at 45 kV and 30 mA. Diffuse reflectance spectra of powder samples were collected using a powdered MgO standard on a Cary 5000 UV−vis spectrophotometer equipped with a "praying mantis" diffuse reflectance accessory. The optical band gaps of different compositions were estimated by extrapolation from Tauc plots of the Kubelka−Munk function $F(R) = (1 - R)^2/2R$, where R is the reflectance.

For ferroelectric testing, both surfaces of polished 0.5 mm thick pellets were coated with silver paste (Heraeus ST601-14) to provide electrical contacts. The ferroelectric switching and hysteresis loops were measured at different frequencies (1−10 Hz) by using a commercial ferroelectric testing system with a high-voltage interface and amplifier (Precision LCII Ferroelectric Test System, Radiant Technologies, Inc.). The samples were immersed in silicone oil in a Teflon sample fixture to prevent the electrical breakdown of air during ferroelectric testing. Devices with an architecture of Si/Ag/ferroelectric layer/ITO were fabricated for the photovoltaic response measurements. One surface of the 0.5 mm pellet was first polished (MultiPrep Polishing System, Allied High Tech Products Inc.) with diamond lapping films and then mounted on a Si wafer with silver epoxy (EPO-TEK H20E, Epoxy Technology, Inc.) which served as the bottom electrode. The top surface of the sample was further polished until the sample thickness reached 30 μm as monitored by a micrometer. The top electrodes comprised arrays of transparent, 200 μm diameter, 150 nm thick pads of indium tin oxide (ITO) patterned by photolithography and evaporated on the top surface at temperatures below 373 K. The devices were poled in a probe station (Lakeshore Cryotronics, Model TTP4) by applying voltage pulses on the ITO pads. After poling, the photovoltaic responses under 405, 450, 532, and 635 nm (Laser Diode Modules, Thorlabs, Inc.) and an AM 1.5 light source (LCS-100 Solar Simulator, Oriel Instruments) were collected by using a semiconductor parameter analyzer (Keithley, Model 4200-SCS).

3. RESULTS AND DISCUSSION

3.1. $PbTiO_3$−$BiFeO_3$ Pseudobinary. The phase stability of the (x)PT−$(1 - x)$BF solid solutions was investigated over the entire range of compositions using XRD (Figure 2a). All compositions showed single-phase perovskite patterns except $BiFeO_3$, which contained small amounts of $Bi_{25}FeO_3$ and $Bi_2Fe_4O_9$ secondary phases (see full scans in Figure S1). At room temperature the solid solution retains a PT-type structure from $0.3 < x < 1.0$, and the tetragonality, as manifested by the splitting of the $(001)_T/(100)_T$ and $(011)_T/(110)_T$ peaks, increased with decreasing x. From the calculated lattice parameters (Table S1), at $x = 0.3$ $c/a = 1.19$, which is consistent with literature data.[60] The compositions with the highest tetragonality (i.e., $x = 0.3$ and 0.325) also form a metastable rhombohedral phase when the particle size is small (⩽1 μm).[61] The details of the stabilization of the different phases are described in Figure S2. For $x \leqslant 0.2$, the tetragonal reflections completely transform to the rhombohedral peaks, $(102)_R$ and $(104)_R/(110)_R$, and as reported previously a region of two-phase coexistence is observed between $0.2 < x < 0.3$.[62]

The optical absorption of the (x)PT−$(1 - x)$BF samples was investigated by diffuse reflectance spectroscopy, and the resultant Kubelka−Munk function $F(R)$ (Figure 2b) contains two principal features. The first is a strong absorption edge followed by a plateau extending up to 6 eV, which is present for all compositions. This excitation, which defines the E_g of (x)PT−$(1 - x)$BF, is caused by charge transfer from the oxygen 2p states at the valence band maximum to the transition metal (e.g., Ti^{4+} or Fe^{3+}) 3d states at the conduction band minimum. The onset of this fundamental absorption edge is red-shifted from ∼3 to 2.2 eV by the substitution of $BiFeO_3$ into $PbTiO_3$. The second feature is the appearance of broad and weak absorption peaks below 2.2 eV for $BiFeO_3$-rich compositions. These result from localized Fe^{3+} d−d transitions due to the crystal field (see Figure S3); they are forbidden by the Laporte rule and do not contribute to the photoconduction.

The fundamental absorption edge of the (x)PT−$(1 - x)$BF spectra was analyzed by using Tauc plots to quantify the magnitude of the direct and indirect optical gap. Details of the line fits for the Tauc plots are provided in Figure S4, and the variation of the optical E_g with x is shown in Figure 2c. The absorption edge of the tetragonal compositions ($x \geqslant 0.3$) is well-fitted by a single allowed direct transition, resulting in a decreased direct E_g as the tetragonality increases. The rhombohedral compositions ($x < 0.3$), especially $BiFeO_3$, show two distinct direct transitions. The first transition at higher energy is in agreement with the frequently reported E_g of 2.7 eV for $BiFeO_3$ films obtained by spectroscopic ellipsometry.[33−35] The second lower energy transition is more likely due to a combination of high energy crystal-field excitations and exciton bands[36,63−65] (see Figures S3 and S4). The tetragonal compositions with $x \geqslant 0.4$ also show a well-defined linear region in the indirect Tauc plot; however, for $x \leqslant 0.3$ the strong overlap of the d−d transitions and the charge transfer absorption edge prevent any satisfactory fitting for an indirect transition. It should be noted that the lowest direct E_g (= 2.18 eV) is observed in the composition ($x = 0.3$) with the highest tetragonality, and the transformation to the rhombohe-

DOI: 10.1021/acs.chemmater.9b00996
Chem. Mater. 2019, 31, 4184−4194

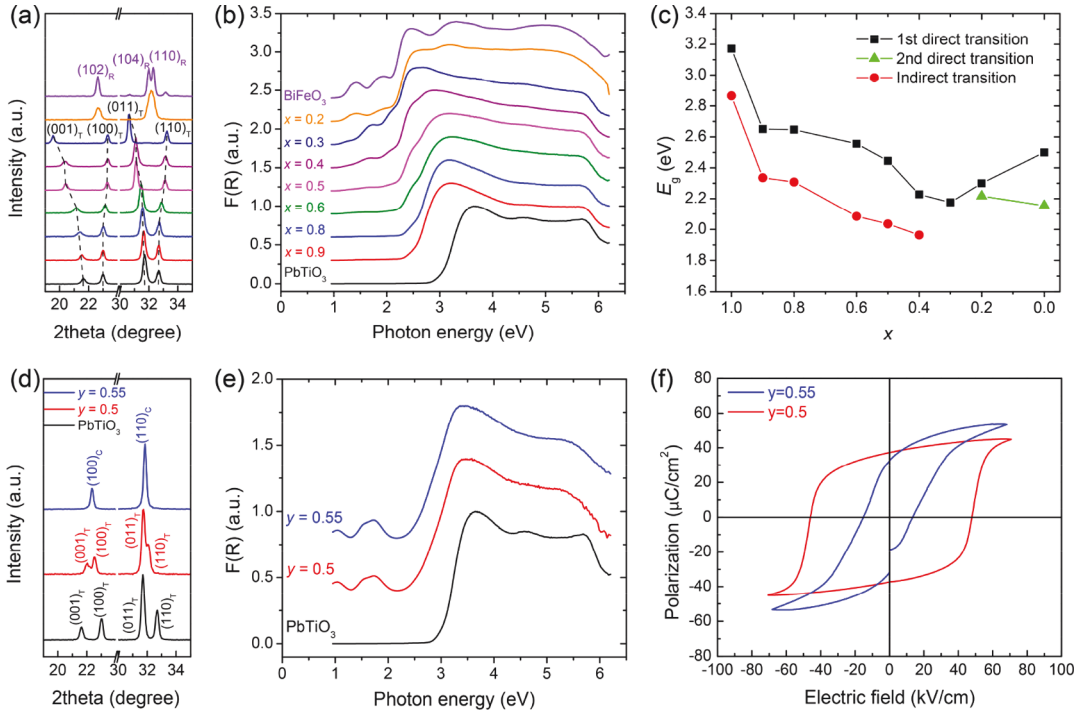

Figure 2. (x)PT−$(1 - x)$BF solid solutions: (a) XRD patterns; (b) Kubelka−Munk spectra; (c) optical band gap. $(1 - y)$PT−(y)BNT solid solutions: (d) XRD patterns; (e) Kubelka−Munk spectra; (f) ferroelectric hysteresis loops measured at 1 Hz.

dral phase fundamentally alters the electronic structure of the (x)PT−$(1 - x)$BF solid solution.

3.2. $PbTiO_3$−$Bi(Ni_{1/2}Ti_{1/2})O_3$ Pseudobinary. $Bi(Ni_{1/2}Ti_{1/2})O_3$ (BNT), which has a balance of ferroelectrically active Ti^{4+} and gap-lowering Ni^{2+} cations on the B-site, was chosen to modify the tetragonal (x)PT−$(1 - x)$BF solid solutions through formation of an MPB. First the $(1 - y)$PT−(y)BNT pseudobinary was explored to quantify the effect of the BNT additive on the structure and ferroelectric and optical properties of lead titanate. The splitting of the $(001)_T/(100)_T$ and $(011)_T/(110)_T$ reflections in the XRD patterns of the solid solution (Figure 2d) is reduced up to $y = 0.5$; their replacement by pseudocubic $(100)_C$ and $(110)_C$ peaks at $y = 0.55$ confirms the previously reported location of the MPB.[57]

The diffuse reflectance spectra (Figure 2e) show the substitution of BNT also causes a shift in the onset of the absorption edge, from 3 eV for pure $PbTiO_3$ to ~2.5 eV for $y = 0.5$ and 0.55; these compositions have almost identical absorption spectra with weaker additional peaks appearing below 2 eV. The weaker peaks are associated with localized d−d transitions for octahedral complexes of Ni^{2+} and can be attributed to $^3A_{2g}$ to $^3T_{2g}$ and $^3A_{2g}$ to $^3T_{1g}$ transitions through a Tanabe−Sugano diagram.[66] The Tauc plots (Figure S5) yield a direct and indirect gap of 2.85 and 2.2 eV for both $y = 0.5$ and 0.55 samples.

In contrast to their similar optical absorption, the ferroelectric response of the $y = 0.5$ and 0.55 ceramics (Figure 2f) are very different, as expected for compositions close to an MPB. Tetragonal $y = 0.5$ has a well-saturated hysteresis loop with a coercive field $(E_c) = 50$ kV/cm and $P_r = 38\ \mu C/cm^2$; the loop for pseudocubic $y = 0.55$ is more slanted with $E_c = 18$ kV/cm and $P_r = 32\ \mu C/cm^2$. The large reduction of E_c at $y = 0.55$ is consistent with the lower barrier to domain switching in the pseudocubic MPB phase.

3.3. $PbTiO_3$−$BiFeO_3$−$Bi(Ni_{1/2}Ti_{1/2})O_3$ Ternary Compositions. The evolution of the MPB in the $PbTiO_3$−$BiFeO_3$−$Bi(Ni_{1/2}Ti_{1/2})O_3$ ternary was investigated by synthesizing samples in the vicinity of the tie line connecting the MPB in the (x)PT−$(1 - x)$BF $(x = 0.27)$ and $(1 - y)$PT−(y)BNT $(y = 0.55)$ pseudobinaries. Compositions were prepared along tie lines from BNT to (x)PT−$(1 - x)$BF with $x = 0.85$, 0.7, 0.5, and 0.325 (Figure 3); the MPB was identified by locating the transition from tetragonal to pseudocubic symmetry in the XRD patterns and from the reduction of E_c in the ferroelectric hysteresis loops (Figure S6). For the $x = 0.325$ tie line the transition from tetragonal to pseudocubic could be observed in the XRD patterns; however, the higher conductivity of the $BiFeO_3$-rich ceramics prevented any significant ferroelectric switching for electric fields up to 70 kV/cm (Figure S6). The difficulty in switching $BiFeO_3$-containing ceramics due to their conductivity and/or domain wall clamping from the ordered alignment of Fe^{2+}−oxygen vacancy defect dipoles has been reported in many other studies.[67−69] The location of the ternary MPB deduced from the structural and ferroelectric responses of the samples is shown in Figure 3a.

The optical absorption properties of the PT−BF−BNT system were analyzed through Tauc plots, and the extracted direct E_g of various compositions is shown in Figure 3b; the corresponding values for an indirect gap are presented in Figure S7. BF and BNT are both effective in reducing the charge transfer gap of the solid solutions, resulting in a continuously tunable E_g ranging from 3.2 to 1.75 eV. The tunability could potentially enable optimization for applications in multijunction solar cells as previously shown in other perovskite oxide[23] and halide systems.[70,71] For the $x = 1$, 0.7, and 0.5 compositional lines, the substitution of BNT into (x)PT−$(1 - x)$BF can further reduce the charge transfer gap through the broadening of the localized Ni 3d e_g states to the conduction band minimum.[72] Along the $x = 0.325$ line the

DOI: 10.1021/acs.chemmater.9b00996
Chem. Mater. 2019, 31, 4184−4194

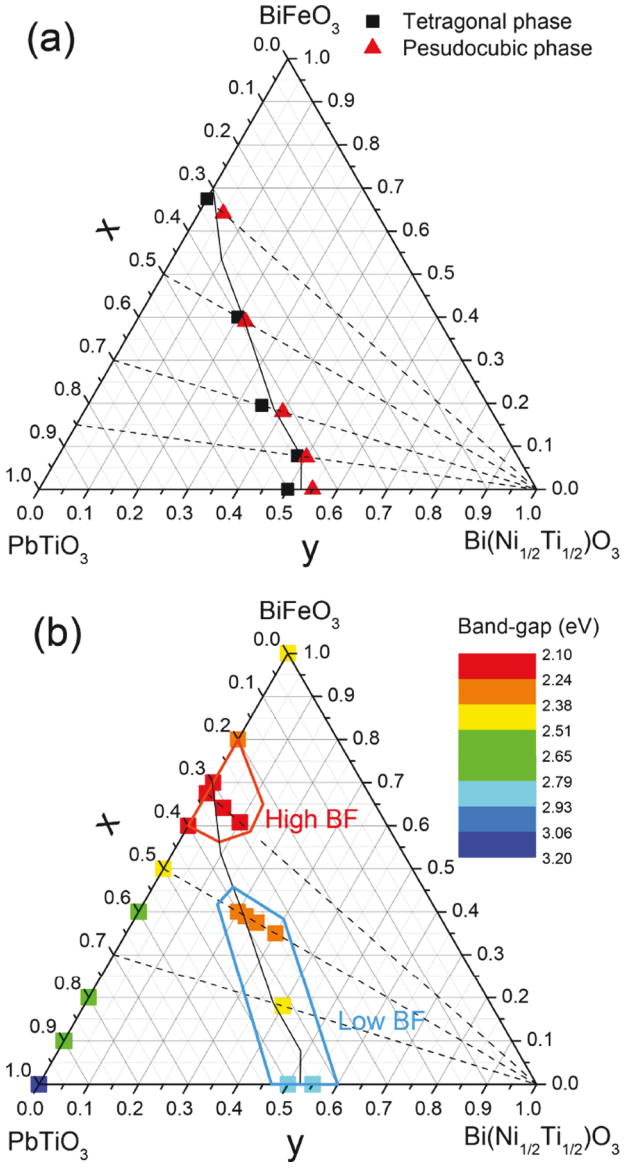

Figure 3. (a) Schematic of the $(1-y)[(x)\mathrm{PT}-(1-x)\mathrm{BF}]-(y)\mathrm{BNT}$ pseudoternary phase diagram. Dashed lines represent tie lines explored to monitor the changes in structure and properties; the resultant MPB is marked by the solid line. Detailed XRD and ferroelectric data along each tie line are provided in Figure S6. (b) Color map of the measured direct band gaps. The MPB regions with high and low BF content are indicated.

increasing BNT content produces a slight blue-shift in the absorption edge (see Figure S8) due to an abrupt change in structure from highly tetragonal to pseudocubic (Figure S6); this increase in the gap is similar to the effect of the structure change on the band gap observed at $x = 0.3$ and 0.325 in the $(x)\mathrm{PT}-(1-x)\mathrm{BF}$ pseudobinary (Figure S2). These observations indicate the MPB in the high and low BF regions marked in Figure 3b are different in terms of the evolution of electronic structures for compositions across the MPB.

Three representative compositions—"A": $(Pb_{0.45}Bi_{0.55})(Ni_{0.275}Ti_{0.725})O_3$ ($x = 1$, $y = 0.55$); "B": $(Pb_{0.42}Bi_{0.58})(Fe_{0.18}Ni_{0.20}Ti_{0.62})O_3$ ($x = 0.7$, $y = 0.4$); and "C": $(Pb_{0.39}Bi_{0.61})(Fe_{0.39}Ni_{0.11}Ti_{0.50})O_3$ ($x = 0.5$, $y = 0.22$)—were selected to investigate the evolution of the structure and properties in the vicinity of the MPB in the pseudoternary (Figure 4a). The XRD patterns, ferroelectric response, and Tauc plots of these MPB compositions are shown in Figures 4b, 4c, and 4d, respectively. The XRD patterns show pseudocubic structures for A and B; composition C has a main pseudocubic phase with a trace amount of a tetragonal structure. The ferroelectric hysteresis loops of the three compositions are well saturated with minimal contributions from conductivity. As the BF content along the MPB increases, E_c also increases while the saturation polarization decreases, indicating the domain switching is harder in $BiFeO_3$-rich compositions. The range of P_r values, 32−39 $\mu C/cm^2$, exceeds those previously reported for compositions lying in the tetragonal phase field of the PT−BF−BNT system.[73] The Tauc plots show a reduction in the direct gap along the MPB with increasing BF content, and this leads to a strong variation in the color of the samples (inset of Figure 4d) from green (A) to red (B) to almost black (C). However, it should be noted that composition B shows the smallest indirect $E_g = 1.75$ eV and the largest difference in the value of the direct and indirect gaps. The combination of a narrow band gap and a large P_r for the ternary PT−BF−BNT MPB compositions compares favorably to those previously reported for other ferroelectric ceramic photovoltaic systems (Figure S9). These MPB compositions also maintain T_C's, ranging from ∼670 to 850 K, that are among the highest reported for a photovoltaic ferroelectric oxide (the dielectric data are provided in Figure S10), potentially allowing high-temperature applications. Their photovoltaic performance is assessed in the following section.

3.4. Photovoltaic Properties of MPB Compositions. *Switchability and Above-Band-Gap V_{oc}.* The photovoltaic properties of the MPB compositions A, B, and C were measured using an ITO/FE-layer/Ag device structure (Figure S11). The electrode materials were deliberately chosen to reduce the difference in the work function of the top and bottom electrodes; the work functions for polycrystalline silver and ITO are ∼4.3 and ∼4.5 eV, respectively.[42] Composition B (direct $E_g = 2.5$ eV; $P_r = 39$ $\mu C/cm^2$) is representative in illustrating the polarization-modulated photovoltaic response under above-band-gap monochromatic illumination (450 nm, ∼50 mW/cm^2) (see Figure S12 for the response of composition C). The sign of the measured current is defined as positive for current flow from the top to bottom electrode through the ferroelectric layer. In the virgin state (i.e., before poling), under zero bias composition B does not shown any significant response with the light on or off (middle panel, Figure 5a) except for a small transient current spike triggered by turning on the laser, which immediately decays to a negligible steady-state photocurrent. The absence of a steady-state current in the virgin state rules out any significant contribution to the photoresponse from ferroelectric imprint effects and/or asymmetrical Schottky barriers.

The sample was then positively poled at 300 K using a 300 s, 200 V step-like voltage pulse. During poling the area under the top electrode showed a clear shape change (Figure S11), indicating a strong electromechanical response in the sample. After positive poling, a significant photocurrent was induced in a direction opposite to the ferroelectric polarization (top panel, Figure 5a). Multiple light on/off cycles gave reproducible patterns for the photocurrent. The same area of the sample was then negatively poled, and in accordance with the switching of the ferroelectric polarization, under the same illumination conditions the polarity of the photocurrent was reversed in a symmetric manner (bottom panel, Figure 5a). The switchable

DOI: 10.1021/acs.chemmater.9b00996
Chem. Mater. 2019, 31, 4184−4194

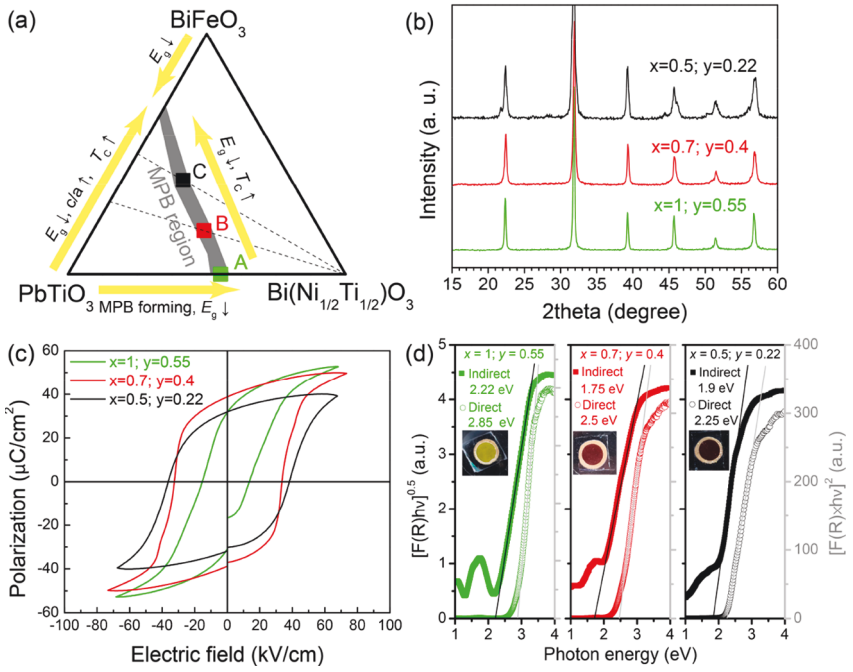

Figure 4. Structure, optical and ferroelectric properties of the MPB compositions selected for detailed investigation in the $(1-y)[(x)\mathrm{PT}-(1-x)\mathrm{BF}]-(y)\mathrm{BNT}$ ternary: (a) locations of compositions A ($x = 1$, $y = 0.55$), B ($x = 0.7$, $y = 0.4$), and C ($x = 0.5$, $y = 0.22$) and a summary of the property variations across the system. (b) XRD patterns. (c) Ferroelectric hysteresis loops. (d) Tauc plots used for band-gap calculations; images of the polished surfaces of each sample are inset.

photoresponse clearly demonstrates the concurrence of the bulk polarization and the photovoltaic effect.

The $I-V$ responses of composition B with up and down polarized states were studied to elucidate the distinct features of the observed photovoltaic effect (Figure 5b). The $I-V$ curves were collected using a slow voltage sweep rate (0.05 V/s) to achieve quasi-steady-state currents at each voltage and minimize hysteresis from the capacitor component of the circuit. The dark $I-V$s of the up and down poled states pass through the origin, and their linear response between ±10 V shows there is no significant contribution from domain back-switching or electromigration of mobile defects, ensuring an equilibrium polarization during the sweep. Under illumination the $I-V$ response of the up/down poled states was quite different than conventional photovoltaics where the built-in electric field inside the heterojunctions and Schottky barriers provides the driving force for carrier separation. First, similar to the photocurrent versus time measurements, the polarity of the $I-V$ curve is switched after reversal of the polarization. Second, the $I-V$ curves of the oppositely poled states are nearly symmetrical with the same absolute value of the open-circuit voltage (6 V), which is equivalent to a photogenerated electric field E_p = 2 kV/cm (below the coercive field E_c = 35 kV/cm), and slightly different absolute values of the short-circuit current (65 and 80 pA for polarization up and down, respectively). The difference can be explained by the polarization-induced modification of the Schottky barriers, which combines with the bulk contribution to produce the overall photovoltaic response. A more detailed analysis of the band bending at the electrode interfaces is provided in the Supporting Information (see Figure S13). Third, the 6 V V_{oc} (obtained from the median value of the forward and reverse sweeps) is multiple times larger than the band gap of the composition (E_g = 2.5 eV), which is not possible in a traditional single junction solar cell. These observations are consistent with the BPVE model in which the built-in electric field is not required for carrier separation and the V_{oc} is not limited by the band gap.

To further clarify the origin of the high open-circuit voltage, it is useful to compare these results to the above-band-gap V_{oc} reported for the nonferroelectric polycrystalline hybrid perovskite $CH_3NH_3PbI_3$. In that system the high V_{oc} has been attributed to the granular nature of the polycrystalline films and the series connection of multiple subcells through intergrain tunneling junctions.[74] The formation of a tunneling junction in $CH_3NH_3PbI_3$ results from the accumulation of a substantial number of mobile charged ions at grain boundaries during poling. However, the likelihood of a significant contribution from a tunneling junction mechanism in our samples is very low as the activation energy for ion migration in perovskite oxides, even those considered as good oxygen conductors, is typically at least 1 order of magnitude higher than the hybrid perovskites.[75,76] This conclusion is supported by additional measurements made at 173 K where a very large above-band-gap V_{oc} = 10 V was observed at a temperature where any ion migration is extremely unlikely during poling (Figure S14). This comparison points to a mechanism where the observed anomalous V_{oc} in PT-BF-BNT devices are caused by the BPVE associated with the absence of crystal inversion symmetry and/or ferroelectric-related boundary effects that do not rely on ion migration.

Wavelength Dependence. To determine how the photoresponse is affected by the evolution of the band gap along the ternary MPB, spectroscopic analyses of the photocurrent under zero bias were conducted on samples A–C under different excitation wavelengths (405, 450, 532, and 635 nm). All samples were poled to a "polarization down" state prior to measurement. Composition A ($x = 1$, $y = 0.55$; direct E_g = 2.85 eV) shows the smallest photoresponse (Figure 6a) due to the larger E_g and partial depolarization as evidenced by the gap in the hysteresis loop (see Figure 4c). In this sample a significant

DOI: 10.1021/acs.chemmater.9b00996
Chem. Mater. 2019, 31, 4184–4194

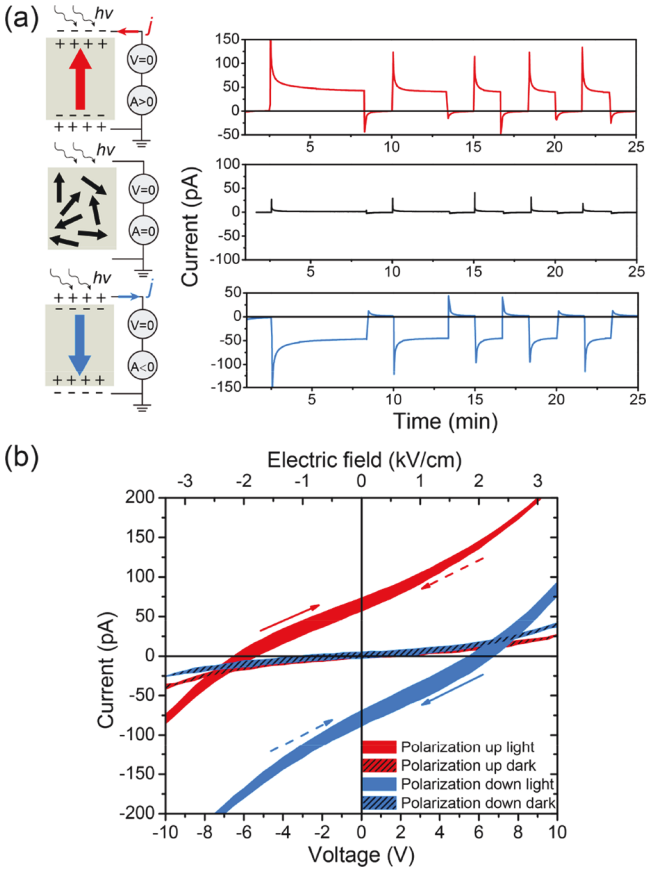

Figure 5. Photoresponse, switchability, and $I-V$ characteristics of composition B ($x = 0.5$, $y = 0.4$) under 450 nm laser illumination. (a) Top: photocurrents for laser on/off cycles after negatively poling (polarization up); middle: nonpoled state; bottom: after positive poling (polarization down). (b) $I-V$ response of oppositely poled states in the dark and under illumination; solid arrows indicate the direction of the forward sweep and dashed arrows the backward sweep.

steady-state photocurrent density (j_{ph}), 0.015 μA/cm^2, was only observed under 450 nm illumination, which is close to the value of the direct gap. Wavelengths below (532 and 635 nm) and above (405 nm) the direct gap produced a transient response that eventually decayed to a negligible steady-state photocurrent (inset of Figure 6a). The transient response was wavelength-dependent, and the spikes for below- and above-band-gap illumination have opposite polarity. In ferroelectric materials, transient photoresponses that eventually equilibrate to steady-state values are frequently attributed to pyroelectric currents originating from the heating of the sample under illumination;[9,77] however, this would not explain the change in the polarity of transient spikes that we observe at the different wavelengths.

The wavelength dependence of the photocurrent is more prominent in compositions B and C, which have a larger P_r and narrower direct E_g. For composition B ($x = 0.7$, $y = 0.4$; direct E_g = 2.5 eV) all wavelengths produce a larger negative j_{ph} (Figure 6b) compared to composition A. The above-band-gap illumination (405 and 450 nm) induced a transient spike which decays to the steady-state current, while the below-band-gap illumination (532 and 635 nm) produced a current that gradually increases to the steady-state value. Considering the change in the polarity of the transient spikes observed for sample A, the photoresponse of composition B can be treated as a superposition of a transient spike which decays to zero and a steady-state step function. The transient is likely related to a surface recombination process,[78] while the steady-state response results from the BPVE.[79] Composition C ($x = 0.5$, $y = 0.22$; direct E_g = 2.25 eV) yielded a similar photoresponse to its sample B counterpart; however, the steady-state currents under long-wavelength illumination (532 and 635 nm) were larger (Figure 6c). The near-band-gap illumination (532 nm) yielded an instantaneous establishment of the largest steady-state j_{ph} (= 0.078 μA/cm^2), consistent with a fast band−band excitation without trapping or thermal activation processes from levels within the band gap.[79] The variation of the photoresponse with wavelength is commonly used as an alternative method for determining the band gaps of semiconductors.[80] The observation of a maximum photoresponse at the absorption edge is not unusual; the decrease in the photoresponse at longer wavelengths is due to the decrease in the excitation of free carriers, while for wavelengths below the maximum the photocurrent is limited by the reduced penetration depth (0.1 μm assuming an absorption coefficient of ~10^5 cm^{-1} for above-band-gap illumination)[33] with the radiation largely being absorbed near the surface where rapid carrier recombination can occur.

If the steady-state photocurrents for the three MPB compositions are plotted as a function of the illumination wavelength (Figure 6d), it is apparent the near-band-gap illumination stimulates the highest response. This is potentially due to the combined result of strong band−band excitation and a good match between the absorption depth and sample thickness for the near-band-gap illumination. Composition C, which has the narrowest direct E_g, generates the largest photocurrent under all the wavelengths used in this study. Furthermore, samples B and C are among the few ferroelectric oxides (e.g., KBNNO[17] and $BiFeO_3$[81,82]) that show a steady-state photovoltaic effect for wavelengths larger than 600 nm.

Performance under 1 sun AM 1.5 G Illumination. The photoresponse of the MPB samples was also measured under 1 sun AM 1.5 G conditions; as expected, the photocurrents (shown in Figure 7a for a "polarization up" state) increase with decreasing band gap. The photovoltaic $I-V$ characteristics of B and C (Figure 7b) were quantified by averaging the forward and reverse sweeps. Both compositions show a linear $I-V$ response with an above-band-gap V_{oc}: for B, V_{oc} = 5.0 V (E_p = 1.7 kV/cm) and j_{sc} = 0.09 μA/cm^2; for C, V_{oc} = 2.6 V (E_p = 0.87 kV/cm) and j_{sc} = 0.11 μA/cm^2. The power conversion efficiencies under 1 sun for B and C are 1.1 × 10^{-4}% and 7.15 × 10^{-5}%, respectively, assuming a fill factor of 0.25 for linear $I-V$. These values compare favorably to most state-of-the-art ferroelectric ceramics due to the coexistence of $P_r \geqslant 32$ μC/cm^2 and a direct $E_g \leqslant 2.5$ eV. For example, the photogenerated electric fields (E_p) for B and C are much higher than those reported for $Ba_{1-x}(Bi_{0.5}Li_{0.5})_xTiO_3$ (E_p = 0.32 kV/cm) where P_r ~10 μC/cm^2,[44] and $(K,Na)NbO_3-Ba(Ni_{0.5}Nb_{0.5})O_{3-\delta}$ (0.27 kV/cm), which has $P_r \approx 11$ μC/cm^2.[47] Similar fields have been reported in $PT-Bi(Ni_{2/3}Nb_{1/3})O_3$ (E_p = 2 kV/cm), another MPB system with a comparable P_r; however, for that system the j_{sc} (~0.04 μA/cm^2) collected under 100 mW/cm^2 white light is more than 50% lower than those we observe for the PT−BF−BNT compositions.[19] The higher j_{sc} for PT−BF−BNT arises from the lower band gaps and highlights the importance of combining a large P_r with a low E_g in optimizing the photovoltaic performance of ferroelectric oxide ceramics.

DOI: 10.1021/acs.chemmater.9b00996
Chem. Mater. 2019, 31, 4184−4194

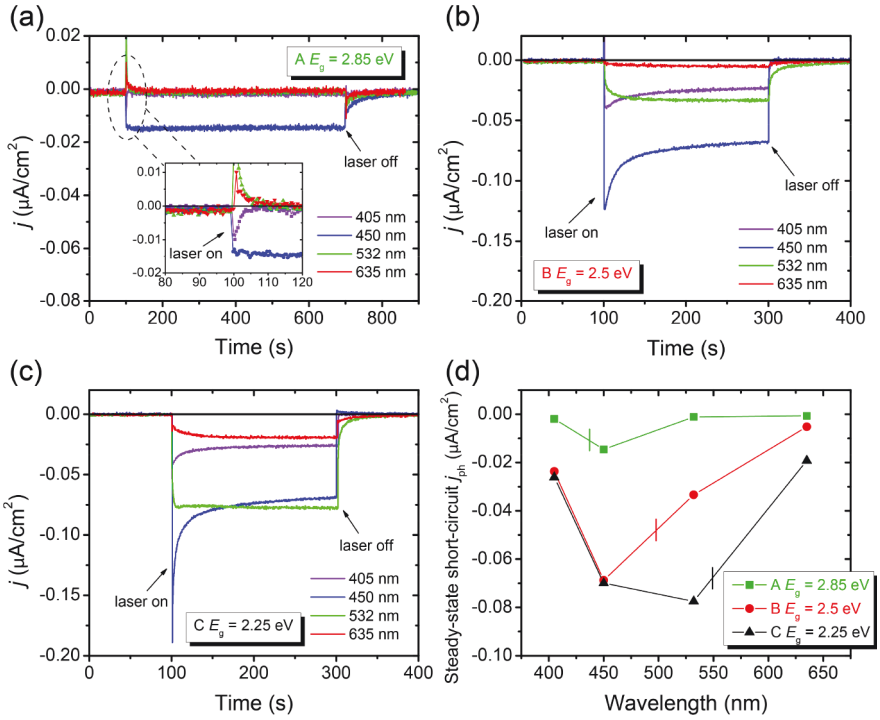

Figure 6. Photoinduced responses of (a) composition A (x = 1, y = 0.55; direct E_g = 2.85 eV), (b) B (x = 0.7, y = 0.4; direct E_g = 2.5 eV), and (c) C (x = 0.5, y = 0.22; direct E_g = 2.26 eV) under monochromatic illumination of various wavelengths. (d) Spectral dependence of steady-state photocurrents of A, B, and C (vertical markers indicate optical band gap of each composition).

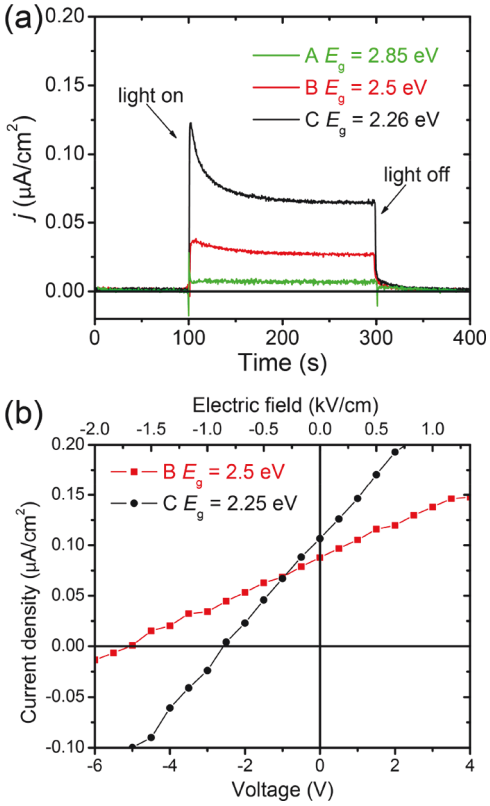

Figure 7. (a) Photoresponses and (b) I–V responses of MPB compositions under 1 sun AM 1.5 G.

4. CONCLUSION

In an attempt to combine a continuous tunability of the band gap while maximizing the ferroelectric polarization, high c/a perovskites along the $PbTiO_3$–$BiFeO_3$ (PT–BF) pseudobinary were modified by substituting an MPB-forming additive, $Bi(Ni_{1/2}Ti_{1/2})O_3$ (BNT), and their photovoltaic properties were explored. Ternary compositions stabilized along the MPB have a direct E_g as low as 2.25 eV (indirect 1.75 eV) and retain a strong ferroelectric polarization (>32 $\mu C/cm^2$) which are advantageous for photovoltaic applications. The BPVE under various wavelengths showed a switchable photoresponse with an above-band-gap V_{oc} (6 V). The reduction of E_g was effective in increasing the short-circuit photocurrent under 1 sun AM 1.5 G conditions. It is possible additional coupling to the piezoelectric properties of these MPB compositions could also enable multisource energy harvesting applications.[47] These results may also guide future optimization of ferroelectric photovoltaics through the growth of their thin film counterparts.

■ ASSOCIATED CONTENT

Supporting Information

The Supporting Information is available free of charge on the ACS Publications website at DOI: 10.1021/acs.chemmater.9b00996.

Full range XRD scans of PT–BF; metastable phases of PT–BF; detailed analysis of absorption spectra for PT–BF; Tauc plots of PT–BF; Tauc plots of PT–BNT; XRD patterns and ferroelectric hysteresis loops of [(x)PT–(1 − x)BF]–BNT tie lines; color map of the indirect band gaps for PT–BF–BNT ternary; absorption spectra of [(x)PT–(1 − x)BF]–BNT tie lines; dielectric measurement of MPB compositions for PT–BF–BNT; pictures of experimental setup; photovoltaic response of composition C; band diagrams of ITO/FE/Ag device; photovoltaic response of composition A at 173 K (PDF)

DOI: 10.1021/acs.chemmater.9b00996
Chem. Mater. 2019, 31, 4184–4194

AUTHOR INFORMATION

Corresponding Author

*E-mail: davies@seas.upenn.edu (P.K.D.).

ORCID

Liyan Wu: 0000-0002-9448-4370

Jonathan E. Spanier: 0000-0002-3096-2644

Present Address

A.P.: The John Hopkins University Applied Physics Laboratory, Laurel, MD.

Notes

The authors declare no competing financial interest.

ACKNOWLEDGMENTS

A.P. and J.E.S. acknowledge support from the ORISE Program of the U.S. Department of Energy under Grant DE-SC0014664 and from the NSF under Grant CBET 1705440. The authors thank Andrew M. Rappe's group from the Department of Chemistry of the University of Pennsylvania for many useful discussions and Cherie R. Kagan's group from the Department of Electrical and System Engineering of the University of Pennsylvania for the use of their UV−vis spectrometer.

REFERENCES

(1) Lines, M. E.; Glass, A. M. *Principles and Applications of Ferroelectrics and Related Materials*; Clarendon Press: Oxford, UK, 1977.

(2) Wang, J.; Neaton, J. B.; Zheng, H.; Nagarajan, V.; Ogale, S. B.; Liu, B.; Viehland, D.; Vaithyanathan, V.; Schlom, D. G.; Waghmare, U. V.; et al. Epitaxial $BiFeO_3$ Multiferroic Thin Film Heterostructures. *Science* **2003**, *299* (5613), 1719−1722.

(3) Kimura, T.; Goto, T.; Shintani, H.; Ishizaka, K.; Arima, T.; Tokura, Y. Magnetic Control of Ferroelectric Polarization. *Nature* **2003**, *426* (6962), 55−58.

(4) Chen, F. S. Optically Induced Change of Refractive Indices in $LiNbO_3$ and $LiTaO_3$. *J. Appl. Phys.* **1969**, *40* (8), 3389−3396.

(5) Fridkin, V. M.; Grekov, A. A.; Ionov, P. V.; Rodin, A. I.; Savchenko, E. A.; Mikhailina, K. A. Photoconductivity in Certain Ferroelectrics. *Ferroelectrics* **1974**, *8* (1), 433−435.

(6) Glass, A. M.; von der Linde, D.; Negran, T. J. High-voltage Bulk Photovoltaic Effect and the Photorefractive Process in $LiNbO_3$. *Appl. Phys. Lett.* **1974**, *25* (4), 233−235.

(7) Kreisel, J.; Alexe, M.; Thomas, P. A. A Photoferroelectric Material Is More than the Sum of Its Parts. *Nat. Mater.* **2012**, *11* (4), 260−260.

(8) Sturman, B. I.; Fridkin, V. M. *Photovoltaic and Photorefractive Effects in Noncentrosymmetric Materials*; Gordon and Breach Science Publishers: Philadelphia, PA, 1992.

(9) Spanier, J. E.; Fridkin, V. M.; Rappe, A. M.; Akbashev, A. R.; Polemi, A.; Qi, Y.; Gu, Z.; Young, S. M.; Hawley, C. J.; Imbrenda, D.; et al. Power Conversion Efficiency Exceeding the Shockley−Queisser Limit in a Ferroelectric Insulator. *Nat. Photonics* **2016**, *10* (9), 611−616.

(10) Yang, S. Y.; Seidel, J.; Byrnes, S. J.; Shafer, P.; Yang, C.-H.; Rossell, M. D.; Yu, P.; Chu, Y.-H.; Scott, J. F.; Ager, J. W.; et al. Above-Bandgap Voltages from Ferroelectric Photovoltaic Devices. *Nat. Nanotechnol.* **2010**, *5* (2), 143−147.

(11) Lee, D.; Baek, S. H.; Kim, T. H.; Yoon, J.-G.; Folkman, C. M.; Eom, C. B.; Noh, T. W. Polarity Control of Carrier Injection at Ferroelectric/Metal Interfaces for Electrically Switchable Diode and Photovoltaic Effects. *Phys. Rev. B: Condens. Matter Mater. Phys.* **2011**, *84* (12), 125305.

(12) Yi, H. T.; Choi, T.; Choi, S. G.; Oh, Y. S.; Cheong, S.-W. Mechanism of the Switchable Photovoltaic Effect in Ferroelectric $BiFeO_3$. *Adv. Mater.* **2011**, *23* (30), 3403−3407.

(13) Gu, Z.; Imbrenda, D.; Bennett-Jackson, A. L.; Falmbigl, M.; Podpirka, A.; Parker, T. C.; Shreiber, D.; Ivill, M. P.; Fridkin, V. M.; Spanier, J. E. Mesoscopic Free Path of Nonthermalized Photogenerated Carriers in a Ferroelectric Insulator. *Phys. Rev. Lett.* **2017**, *118* (9), 096601.

(14) Burger, A. M.; Agarwal, R.; Aprelev, A.; Schruba, E.; Gutierrez-Perez, A.; Fridkin, V. M.; Spanier, J. E. Direct Observation of Shift and Ballistic Photovoltaic Currents. *Sci. Adv.* **2019**, *5* (1), No. eaau5588.

(15) Alexe, M.; Hesse, D. Tip-Enhanced Photovoltaic Effects in Bismuth Ferrite. *Nat. Commun.* **2011**, *2* (1), 256.

(16) Bhatnagar, A.; Roy Chaudhuri, A.; Heon Kim, Y.; Hesse, D.; Alexe, M. Role of Domain Walls in the Abnormal Photovoltaic Effect in $BiFeO_3$. *Nat. Commun.* **2013**, *4* (1), 2835.

(17) Grinberg, I.; West, D. V.; Torres, M.; Gou, G.; Stein, D. M.; Wu, L.; Chen, G.; Gallo, E. M.; Akbashev, A. R.; Davies, P. K.; et al. Perovskite Oxides for Visible-Light-Absorbing Ferroelectric and Photovoltaic Materials. *Nature* **2013**, *503* (7477), 509−512.

(18) Choi, W. S.; Chisholm, M. F.; Singh, D. J.; Choi, T.; Jellison, G. E.; Lee, H. N. Wide Bandgap Tunability in Complex Transition Metal Oxides by Site-Specific Substitution. *Nat. Commun.* **2012**, *3* (1), 689.

(19) Liu, H.; Chen, J.; Ren, Y.; Zhang, L.; Pan, Z.; Fan, L.; Xing, X. Large Photovoltage and Controllable Photovoltaic Effect in $PbTiO_3$-$Bi(Ni_{2/3+x}Nb_{1/3-x})O_{3-\delta}$ Ferroelectrics. *Adv. Electron. Mater.* **2015**, *1* (4), 1400051.

(20) Wu, M.; Lou, X.; Li, T.; Li, J.; Wang, S.; Li, W.; Peng, B.; Gou, G. Ni-Doped $SrBi_2Nb_2O_9$− Perovskite Oxides with Reduced Band Gap and Stable Ferroelectricity for Photovoltaic Applications. *J. Alloys Compd.* **2017**, *724*, 1093−1100.

(21) Wu, L.; Akbashev, A. R.; Podpirka, A. A.; Spanier, J. E.; Davies, P. K. Infrared-to-Ultraviolet Light-Absorbing $BaTiO_3$-Based Ferroelectric Photovoltaic Materials. *J. Am. Ceram. Soc.* **2019**, *102* (7), 4188−4199.

(22) Qi, T.; Grinberg, I.; Rappe, A. M. Band-Gap Engineering via Local Environment in Complex Oxides. *Phys. Rev. B: Condens. Matter Mater. Phys.* **2011**, *83* (22), 224108.

(23) Nechache, R.; Harnagea, C.; Li, S.; Cardenas, L.; Huang, W.; Chakrabartty, J.; Rosei, F. Bandgap Tuning of Multiferroic Oxide Solar Cells. *Nat. Photonics* **2015**, *9* (1), 61−67.

(24) Gou, G.; Charles, N.; Shi, J.; Rondinelli, J. M. A-Site Ordered Double Perovskite $CaMnTi_2O_6$ as a Multifunctional Piezoelectric and Ferroelectric-Photovoltaic Material. *Inorg. Chem.* **2017**, *56* (19), 11854−11861.

(25) Berger, R. F.; Neaton, J. B. Computational Design of Low-Band-Gap Double Perovskites. *Phys. Rev. B: Condens. Matter Mater. Phys.* **2012**, *86* (16), 165211.

(26) Han, H.; Song, S.; Lee, J. H.; Kim, K. J.; Kim, G. W.; Park, T.; Jang, H. M. Switchable Photovoltaic Effects in Hexagonal Manganite Thin Films Having Narrow Band Gaps. *Chem. Mater.* **2015**, *27* (21), 7425−7432.

(27) Huang, X.; Paudel, T. R.; Dong, S.; Tsymbal, E. Y. Hexagonal Rare-Earth Manganites as Promising Photovoltaics and Light Polarizers. *Phys. Rev. B: Condens. Matter Mater. Phys.* **2015**, *92* (12), 125201.

(28) Han, H.; Kim, D.; Chu, K.; Park, J.; Nam, S. Y.; Heo, S.; Yang, C. H.; Jang, H. M. Enhanced Switchable Ferroelectric Photovoltaic Effects in Hexagonal Ferrite Thin Films via Strain Engineering. *ACS Appl. Mater. Interfaces* **2018**, *10* (2), 1846−1853.

(29) Zhang, G.; Wu, H.; Li, G.; Huang, Q.; Yang, C.; Huang, F.; Liao, F.; Lin, J. New High T(c) Multiferroics $KBiFe_2O_5$ with Narrow Band Gap and Promising Photovoltaic Effect. *Sci. Rep.* **2013**, *3*, 1265.

(30) Zhang, G.; Liu, F.; Gu, T.; Zhao, Y.; Li, N.; Yang, W.; Feng, S. Enhanced Ferroelectric and Visible-Light Photoelectric Properties in Multiferroic $KBiFe_2O_5$ via Pressure-Induced Phase Transition. *Adv. Electron. Mater.* **2017**, *3* (3), 1600498.

(31) Van Aken, B. B.; Palstra, T. T. M.; Filippetti, A.; Spaldin, N. A. The Origin of Ferroelectricity in Magnetoelectric $YMnO_3$. *Nat. Mater.* **2004**, *3* (3), 164−170.

(32) Bennett, J. W.; Grinberg, I.; Rappe, A. M. New Highly Polar Semiconductor Ferroelectrics through d^8 Cation-O Vacancy Sub-

DOI: 10.1021/acs.chemmater.9b00996
Chem. Mater. 2019, 31, 4184−4194

stitution into $PbTiO_3$: A Theoretical Study. *J. Am. Chem. Soc.* **2008**, *130* (51), 17409−17412.
(33) Xu, X. S.; Brinzari, T. V.; Lee, S.; Chu, Y. H.; Martin, L. W.; Kumar, A.; McGill, S.; Rai, R. C.; Ramesh, R.; Gopalan, V.; et al. Optical Properties and Magnetochromism in Multiferroic $BiFeO_3$. *Phys. Rev. B: Condens. Matter Mater. Phys.* **2009**, *79* (13), 134425.
(34) Weis, R. S.; Gaylord, T. K. Lithium Niobate: Summary of Physical Properties and Crystal Structure. *Appl. Phys. A: Solids Surf.* **1985**, *37* (4), 191−203.
(35) Ihlefeld, J. F.; Podraza, N. J.; Liu, Z. K.; Rai, R. C.; Xu, X.; Heeg, T.; Chen, Y. B.; Li, J.; Collins, R. W.; Musfeldt, J. L.; et al. Optical Band Gap of $BiFeO_3$ Grown by Molecular-Beam Epitaxy. *Appl. Phys. Lett.* **2008**, *92* (14), 142908.
(36) You, L.; Zheng, F.; Fang, L.; Zhou, Y.; Tan, L. Z.; Zhang, Z.; Ma, G.; Schmidt, D.; Rusydi, A.; Wang, L.; et al. Enhancing Ferroelectric Photovoltaic Effect by Polar Order Engineering. *Sci. Adv.* **2018**, *4* (7), No. eaat3438.
(37) Machado, P.; Scigaj, M.; Gazquez, J.; Rueda, E.; Sánchez-Díaz, A.; Fina, I.; Gibert-Roca, M.; Puig, T.; Obradors, X.; Campoy-Quiles, M.; et al. Band Gap Tuning of Solution-Processed Ferroelectric Perovskite $BiFe_{1-x}Co_xO_3$ Thin Films. *Chem. Mater.* **2019**, *31* (3), 947−954.
(38) Zhang, L.; Chen, J.; Fan, L.; Pan, Z.; Wang, J.; Ibrahim, K.; Tian, J.; Xing, X. Enhanced Switchable Photovoltaic Response and Ferromagnetic of Co-Doped $BiFeO_3$ Based Ferroelectric Thin Films. *J. Alloys Compd.* **2018**, *742*, 351−355.
(39) Liu, F.; Fina, I.; Gutiérrez, D.; Radaelli, G.; Bertacco, R.; Fontcuberta, J. Selecting Steady and Transient Photocurrent Response in $BaTiO_3$ Films. *Adv. Electron. Mater.* **2015**, *1* (9), 1500171.
(40) Kooriyattil, S.; Katiyar, R. K.; Pavunny, S. P.; Morell, G.; Katiyar, R. S. Photovoltaic Properties of Aurivillius Phase $Bi_5FeTi_3O_{15}$ Thin Films Grown by Pulsed Laser Deposition. *Appl. Phys. Lett.* **2014**, *105* (7), No. 072908.
(41) An, H.; Han, J. Y.; Kim, B.; Song, J.; Jeong, S. Y.; Franchini, C.; Bark, C. W.; Lee, S. Large Enhancement of the Photovoltaic Effect in Ferroelectric Complex Oxides through Bandgap Reduction. *Sci. Rep.* **2016**, *6* (1), 28313.
(42) Zhang, J.; Su, X.; Shen, M.; Dai, Z.; Zhang, L.; He, X.; Cheng, W.; Cao, M.; Zou, G. Enlarging Photovoltaic Effect: Combination of Classic Photoelectric and Ferroelectric Photovoltaic Effects. *Sci. Rep.* **2013**, *3*, 2109.
(43) Uchino, K.; Miyazawa, Y.; Nomura, S. Photovoltaic Effect in Ferroelectric Ceramics and Its Applications. *Jpn. J. Appl. Phys.* **1983**, *22* (S2), 102.
(44) Pal, S.; Swain, A. B.; Biswas, P. P.; Murali, D.; Pal, A.; Nanda, B. R. K.; Murugavel, P. Giant Photovoltaic Response in Band Engineered Ferroelectric Perovskite. *Sci. Rep.* **2018**, *8* (1), 8005.
(45) Das, S.; Ghara, S.; Mahadevan, P.; Sundaresan, A.; Gopalakrishnan, J.; Sarma, D. D. Designing a Lower Band Gap Bulk Ferroelectric Material with a Sizable Polarization at Room Temperature. *ACS Energy Lett.* **2018**, *3* (5), 1176−1182.
(46) Hawley, C. J.; Wu, L.; Xiao, G.; Grinberg, I.; Rappe, A. M.; Davies, P. K.; Spanier, J. E. Structural and Ferroelectric Phase Evolution in $[KNbO3]_{1-x}[BaNi_{1/2}Nb_{1/2}O_{3-\delta}]_x$ (x = 0, 0.1). *Phys. Rev. B: Condens. Matter Mater. Phys.* **2017**, *96* (5), No. 054117.
(47) Bai, Y.; Tofel, P.; Palosaari, J.; Jantunen, H.; Juuti, J. A Game Changer: A Multifunctional Perovskite Exhibiting Giant Ferroelectricity and Narrow Bandgap with Potential Application in a Truly Monolithic Multienergy Harvester or Sensor. *Adv. Mater.* **2017**, *29* (29), 1700767.
(48) Suchomel, M. R.; Davies, P. K. Enhanced Tetragonality in $(x)PbTiO_3$-$(1-x)Bi(Zn_{1/2}Ti_{1/2})O_3$ and Related Solid Solution Systems. *Appl. Phys. Lett.* **2005**, *86* (26), 262905.
(49) Stein, D. M.; Suchomel, M. R.; Davies, P. K. Enhanced Tetragonality in $(x)PbTiO_3$-$(1-x)Bi(B'B'')O_3$ Systems: $Bi(Zn_{3/4}W_{1/4})O_3$. *Appl. Phys. Lett.* **2006**, *89* (13), 132907.
(50) Grinberg, I.; Suchomel, M. R.; Davies, P. K.; Rappe, A. M. Predicting Morphotropic Phase Boundary Locations and Transition Temperatures in Pb- and Bi-Based Perovskite Solid Solutions from Crystal Chemical Data and First-Principles Calculations. *J. Appl. Phys.* **2005**, *98* (9), No. 094111.
(51) Pan, Z.; Chen, J.; Yu, R.; Patra, L.; Ravindran, P.; Sanson, A.; Milazzo, R.; Carnera, A.; Hu, L.; Wang, L.; et al. Large Negative Thermal Expansion Induced by Synergistic Effects of Ferroelectrostriction and Spin Crossover in $PbTiO_3$-Based Perovskites. *Chem. Mater.* **2019**, *31* (4), 1296−1303.
(52) Narayan, B.; Adhikari, S.; Madras, G.; Ranjan, R. Trapping a Metastable Ferroelectric Phase by Size Reduction in Semiconducting Ferroelectric $BiFeO_3$-$PbTiO_3$ and Its Implications for Photocatalytic Response. *Phys. Rev. Appl.* **2017**, *7* (2), No. 024018.
(53) Suchomel, M. R. Greater Functionality of Bismuth and Lead Based Perovskites. Ph.D. Thesis, University of Pennsylvania, Philadelphia, PA, 2005.
(54) Gou, G. Y.; Bennett, J. W.; Takenaka, H.; Rappe, A. M. Post Density Functional Theoretical Studies of Highly Polar Semiconductive $Pb(Ti_{1-x}Ni_x)O_{3-x}$ Solid Solutions: Effects of Cation Arrangement on Band Gap. *Phys. Rev. B: Condens. Matter Mater. Phys.* **2011**, *83* (20), 205115.
(55) Zhu, J.; Feng, S.; Liu, Q.; Zhang, J.; Xu, H.; Li, Y.; Li, X.; Liu, J.; Huang, Q.; Zhao, Y.; et al. Temperature and Pressure Effects of Multiferroic Bi_2NiTiO_6 Compound. *J. Appl. Phys.* **2013**, *113* (14), 143514.
(56) Takenaka, T.; Yamada, M. Solid-Solution $(Bi_{1-x}Pb_x)(Ni_{(1-x)/2}Ti_{(1+x)/2})O_3$ for New Piezoelectric Ceramics. *Jpn. J. Appl. Phys.* **1993**, *32*, 4218−4222.
(57) Choi, S. M.; Stringer, C. J.; Shrout, T. R.; Randall, C. A. Structure and Property Investigation of a Bi-Based Perovskite Solid Solution: $(1-x)Bi(Ni_{1/2}Ti_{1/2})O_3-xPbTiO_3$. *J. Appl. Phys.* **2005**, *98* (3), No. 034108.
(58) Zhang, Q.; Jiang, M.; Li, Z. Structural and Dielectric Properties of $(1-x)Bi(Ni_{1/2}Ti_{1/2})O_3$-$xPbTiO_3$ Ceramics with the Morphotropic Phase Boundary Composition. *J. Electroceram.* **2012**, *29* (3), 179−182.
(59) Hu, P.; Chen, J.; Deng, J.; Xing, X. Thermal Expansion, Ferroelectric and Magnetic Properties in $(1-x)PbTiO_3-xBi(Ni_{1/2}Ti_{1/2})O_3$. *J. Am. Chem. Soc.* **2010**, *132* (6), 1925−1928.
(60) Comyn, T. P.; Stevenson, T.; Al-Jawad, M.; Turner, S. L.; Smith, R. I.; Marshall, W. G.; Bell, A. J.; Cywinski, R. Phase-Specific Magnetic Ordering in $BiFeO_3$-$PbTiO_3$. *Appl. Phys. Lett.* **2008**, *93* (23), 232901.
(61) Kothai, V.; Narayan, B.; Brajesh, K.; Kaushik, S. D.; Siruguri, V.; Ranjan, R. Ferroelectric Phase Coexistence by Crystallite Size Reduction in $BiFeO_3-PbTiO_3$. *Phys. Rev. B: Condens. Matter Mater. Phys.* **2014**, *90* (15), 155115.
(62) Kothai, V.; Prasath Babu, R.; Ranjan, R. Metastable Morphotropic Phase Boundary State in the Multiferroic $BiFeO_3-PbTiO_3$. *J. Appl. Phys.* **2013**, *114* (11), 114102.
(63) Ramirez, M. O.; Kumar, A.; Denev, S. A.; Podraza, N. J.; Xu, X. S.; Rai, R. C.; Chu, Y. H.; Seidel, J.; Martin, L. W.; Yang, S.-Y.; et al. Magnon Sidebands and Spin-Charge Coupling in Bismuth Ferrite Probed by Nonlinear Optical Spectroscopy. *Phys. Rev. B: Condens. Matter Mater. Phys.* **2009**, *79* (22), 224106.
(64) Pisarev, R. V.; Moskvin, A. S.; Kalashnikova, A. M.; Rasing, T. Charge Transfer Transitions in Multiferroic $BiFeO_3$ and Related Ferrite Insulators. *Phys. Rev. B: Condens. Matter Mater. Phys.* **2009**, *79* (23), 235128.
(65) Scafetta, M. D.; Cordi, A. M.; Rondinelli, J. M.; May, S. J. Band Structure and Optical Transitions in $LaFeO_3$: Theory and Experiment. *J. Phys.: Condens. Matter* **2014**, *26* (50), 505502.
(66) González, E.; Rodrigue-Witchel, A.; Reber, C. Absorption Spectroscopy of Octahedral Nickel(II) Complexes: A Case Study of Interactions between Multiple Electronic Excited States. *Coord. Chem. Rev.* **2007**, *251* (3−4), 351−363.
(67) Fernández-Posada, C. M.; Castro, A.; Kiat, J.-M.; Porcher, F.; Peña, O.; Algueró, M.; Amorín, H. A Novel Perovskite Oxide Chemically Designed to Show Multiferroic Phase Boundary with

DOI: 10.1021/acs.chemmater.9b00996
Chem. Mater. 2019, 31, 4184−4194

Room-Temperature Magnetoelectricity. *Nat. Commun.* **2016**, *7* (1), 12772.
(68) Amorín, H.; Correas, C.; Fernández-Posada, C. M.; Peña, O.; Castro, A.; Algueró, M. Multiferroism and Enhancement of Material Properties across the Morphotropic Phase Boundary of BiFeO3-$PbTiO_3$. *J. Appl. Phys.* **2014**, *115* (10), 104104.
(69) Amorín, H.; Correas, C.; Ramos, P.; Hungría, T.; Castro, A.; Algueró, M. Very High Remnant Polarization and Phase-Change Electromechanical Response of $BiFeO_3$-$PbTiO_3$ at the Multiferroic Morphotropic Phase Boundary. *Appl. Phys. Lett.* **2012**, *101* (17), 172908.
(70) Noh, J. H.; Im, S. H.; Heo, J. H.; Mandal, T. N.; Seok, S., II Chemical Management for Colorful, Efficient, and Stable Inorganic−Organic Hybrid Nanostructured Solar Cells. *Nano Lett.* **2013**, *13* (4), 1764−1769.
(71) Eperon, G. E.; Stranks, S. D.; Menelaou, C.; Johnston, M. B.; Herz, L. M.; Snaith, H. J. Formamidinium Lead Trihalide: A Broadly Tunable Perovskite for Efficient Planar Heterojunction Solar Cells. *Energy Environ. Sci.* **2014**, *7* (3), 982.
(72) Niedermeier, C. A.; Råsander, M.; Rhode, S.; Kachkanov, V.; Zou, B.; Alford, N.; Moram, M. A. Band Gap Bowing in $Ni_xMg_{1-x}O$. *Sci. Rep.* **2016**, *6* (1), 31230.
(73) Hu, P.; Kang, H.; Chen, J.; Deng, J.; Xing, X. Magnetic Enhancement and Low Thermal Expansion of (1−x−y)$PbTiO_3$-x$Bi(Ni_{1/2}Ti_{1/2})O_3$-y$BiFeO_3$. *J. Mater. Chem.* **2011**, *21* (40), 16205.
(74) Yuan, Y.; Li, T.; Wang, Q.; Xing, J.; Gruverman, A.; Huang, J. Anomalous Photovoltaic Effect in Organic-Inorganic Hybrid Perovskite Solar Cells. *Sci. Adv.* **2017**, *3* (3), No. e1602164.
(75) Cherry, M.; Islam, M. S.; Catlow, C. R. A. Oxygen Ion Migration in Perovskite-Type Oxides. *J. Solid State Chem.* **1995**, *118* (1), 125−132.
(76) Azpiroz, J. M.; Mosconi, E.; Bisquert, J.; De Angelis, F. Defect Migration in Methylammonium Lead Iodide and Its Role in Perovskite Solar Cell Operation. *Energy Environ. Sci.* **2015**, *8* (7), 2118−2127.
(77) Chynoweth, A. G. Surface Space-Charge Layers in Barium Titanate. *Phys. Rev.* **1956**, *102* (3), 705−714.
(78) Peter, L. M. Energetics and Kinetics of Light-Driven Oxygen Evolution at Semiconductor Electrodes: The Example of Hematite. *J. Solid State Electrochem.* **2013**, *17* (2), 315−326.
(79) Alexe, M. Local Mapping of Generation and Recombination Lifetime in $BiFeO_3$ Single Crystals by Scanning Probe Photoinduced Transient Spectroscopy. *Nano Lett.* **2012**, *12* (5), 2193−2198.
(80) Bube, R. H. *Photoconductivity of Solids*; Wiley: New York, 1960.
(81) Yang, M.; Bhatnagar, A.; Alexe, M. Electronic Origin and Tailoring of Photovoltaic Effect in $BiFeO_3$ Single Crystals. *Adv. Electron. Mater.* **2015**, *1* (11), 1500139.
(82) Ge, C.; Jin, K. J.; Zhang, Q. H.; Du, J. Y.; Gu, L.; Guo, H. Z.; Yang, J. T.; Gu, J. X.; He, M.; Xing, J.; et al. Toward Switchable Photovoltaic Effect via Tailoring Mobile Oxygen Vacancies in Perovskite Oxide Films. *ACS Appl. Mater. Interfaces* **2016**, *8* (50), 34590−34597.

DOI: 10.1021/acs.chemmater.9b00996
Chem. Mater. 2019, 31, 4184−4194